# Influence of upstream turbulence on the wake characteristics of a tidal stream turbine

Mohammad H. B. Ahmadi

*Department of Mechanical Engineering and the Built Environment, University of Derby, Derby, DE2 3AW, UK*

**Abstract**

The influence of the upstream turbulence intensity on the flow characteristics downstream of a laboratory-scale horizontal axis tidal stream turbine is investigated in this study. Three test cases with the same mean velocity and different turbulence intensities are simulated numerically using the hybrid large eddy simulation/actuator line modelling technique. The mean velocity components, mean turbulent fluctuations, velocity deficit and wake extension are compared along the streamwise direction to examine the upstream turbulence effects. The inflow conditions are generated by the mapping method using the mean velocity and turbulent profiles experimentally obtained for a turbulent open channel flow. Comparing results for the mean velocity and turbulent fluctuations shows that the upstream turbulence level strongly affects the flow characteristics downstream of the turbine by influencing the tip vortices breakdown process and in turn wake recovery. The comparison also reveals that the ambient turbulence level strongly influences the velocity deficit but it does not significantly affect the streamwise velocity and the radial location of tip vortices in the flow.

*Keywords:* Tidal turbines, ALM, LES, Turbulence, Wake recovery, Wake extension

## 1. Introduction

The upstream turbulence intensity (UTI) plays a key role in the behaviour of horizontal axis Tidal Stream Turbines (TST). The turbulent flow approaching the turbines induces continuous changes on their blade loading and power extraction and deeply influences wake characteristics by affecting the mixing between the wake and the surrounding flow. It may affect various aspects of the wake including wake recovery and tip vortex generation and breakdown. In tidal turbine arrays, the flow approaching downstream turbines will be determined by the far wake of turbines positioned upstream and thus the wake of an upstream turbine may inevitably influence the power performance of another downstream turbine. This implies that for more accurate predictions of array performance and optimisation of tidal arrays, a thorough understanding of the upstream turbulence effects on the turbine wake is a crucial issue.

The influence of UTI on the flow characteristics downstream of tidal turbines have been investigated numerically and experimentally. Myers *et al.* [1] showed the close proximity of the water surface has a

*Email address:* m.ahmadi@derby.ac.uk (Mohammad H. B. Ahmadi)

significant effect on the flow structure behind the turbine. Maganga *et al.* [2] studied the influence of the ambient turbulence intensity on the turbine performance and wake characterization. Myers & Bahaj [3] measured farfield velocities downstream of a porous disc turbine. Both experiments showed that increasing upstream turbulence increased wake recovery. Chamorro *et al.* [4, 5] examined the effects of upstream turbulence and energetic coherent motions on turbine response and their effects on wake recovery. They showed the response is coupled to upstream turbulence below a critical rotation frequency and uncoupled at higher frequencies and wake recovery was related to the tip vortices breakdown and generated large motions. Mycek *et al.* [6, 7] studied the turbulence intensity effects on marine current turbines behaviour; single and two interacting turbines. They showed, while the mean turbine performance remains stable in time, the performance fluctuations dramatically increase with the turbulence intensity. Their work also showed that the wake shape, length and strength largely depend on the upstream turbulence level. Stallard *et al.* [8] studied the mean wake characteristics of an axial turbine in a wide flume to minimise restriction to transverse wake development and behaviour of large-scale horizontal turbulence structures. Blackmore *et al.* [9] numerically investigated the effects of turbulence intensity and integral length scale on the wake behind a gridded actuator disc using an LES model. They concluded marine current turbine arrays could be further optimized, increasing the energy yield of the array when the site-specific turbulence characteristics are considered.

There have also been many studies in this scope for wind turbines which include computational studies by Churchfield *et al.* [10] and Wu & Porte-Agel [11] and experimental works by Hu *et al.* [12] and Zhang *et al.* [13] among others. Turbine loading characteristics and various wake details including tip vortex generation and break down and large scale wake meandering have been analysed in their works.

The previous studies consider a time-invariant mean value for the inflow. Li *et al.* [14] investigated the tidal-cycle variation of tidal flow and the effects of salinity and temperature stratification and showed how the mean velocity, salinity, and turbulence characteristics vary during a tidal cycle. These effects are important in understanding the performance of tidal turbine arrays and how turbine wakes develop. The current study does not aim to consider all characteristics of tidal flows. The effects of density stratification, tidal channel topography, tidal-cycle flow variation and free surface effects are not included here and will be examined in the future work.

The numerical simulation of TSTs allows examination of the flow characteristics just behind the turbine, especially in the transition region, whilst due to practical restrictions is absent in most experimental data. This study aims to investigate the influence of upstream turbulence on the wake recovery and flow characteristics downstream of a tidal turbine by addressing velocity deficit, turbulence intensity, turbulent kinetic energy and wake extension. A laboratory scale 3-bladed horizontal axis turbine is numerically simulated using the hybrid Large Eddy Simulation/Actuator Line Modelling (LES/ALM) technique for three test cases with the same mean velocity profiles and different turbulence intensities on the upstream boundary. The hybrid LES/ALM technique used here has been validated and correlated well with the experimental measurements in previous works [15, 16, 17]. The inflow conditions are generated by the mapping method using the mean

velocity and turbulent profiles obtained for a turbulent open channel flow.

## 2. Numerical modelling

### *2.1. Large eddy simulation*

In LES, the governing equations are obtained by filtering the time-dependent Navier-Stokes equations in physical space, such that those eddies which are below a certain size are filtered out. The resulting equations thus only govern the dynamics of the large scales, although the smaller scales are usually modelled by some eddy-viscosity-based sub-grid scale (SGS) models. Here the turbine geometry is not resolved (i.e. a grid is not fitted around the blades and the support structure). Rather, the actuator lines are used in which the forces created by the turbine are modelled and applied to the flow field as a body force.

The filtered incompressible Navier-Stokes equations in velocity-pressure variables are written as

$$\frac{\partial \bar{u}_i}{\partial x_i} = 0 \tag{1}$$
$$\frac{\partial \bar{u}_i}{\partial t} + \frac{\partial (\bar{u}_i \bar{u}_j)}{\partial x_j} = -\frac{1}{\rho}\frac{\partial \bar{p}}{\partial x_i} + \nu \frac{\partial^2 \bar{u}_i}{\partial x_j^2} + \frac{\partial \tau_{ij}}{\partial x_j} + f_{i,\epsilon}$$

where the bar denotes filtering and $f_{i,\epsilon}$ is the body force provided from the actuator line modelling described briefly in section. 2.2 The turbulent stresses are modelled with an eddy viscosity as

$$\tau_{ij} = -\nu_t \left( \frac{\partial \bar{u}_i}{\partial x_j} + \frac{\partial \bar{u}_j}{\partial x_i} \right) + \frac{2}{3} k \delta_{ij} \tag{2}$$

The eddy viscosity and sub-grid kinetic energy in Eq.(2) are determined using the one-equation eddy viscosity model with solving an extra equation for the sub-grid turbulent kinetic energy [18]. The filtered governing equations are solved using the CFD code library OpenFOAM [19].

### *2.2. Actuator line modelling*

In this study, the geometry of the turbine is not resolved and instead, the turbine is represented using the ALM technique originally developed by Sørensen & Shen [20]. In the ALM technique, the tidal turbine blades are modelled using body forces distributed along rotating lines instead of resolving true geometry of blades. In this method, initially, full 3D Navier-Stokes equations are solved to predict the flow field. Having the flow field together with the blade geometry and tabulated 2D airfoil data, a blade element approach is used to calculate the forces associated to the turbine blades. The calculated 2D forces are corrected for 3D rotational effects using the correction factor introduced by Shen *et al.* [21]. To avoid singular behaviour and numerical instability, the modelled blade forces are distributed smoothly on several mesh points along and away from the actuator lines using a 3D Gaussian projection. In this study, the Gaussian smearing parameter takes a value between 2 and 3 cell sizes [22]. The reader is referred to [16, 17] for a detailed description of the ALM technique used in the present work. The author has briefly explained some advantages and disadvantages of the ALM technique in comparison to other methods in [16, 17]. For a comprehensive review see [23, 24, 25].

### 2.3. Computational domain

In this study, a horizontal axis laboratory scale TST consisting of three blades has been numerically simulated with the hybrid LES/ALM technique for three inflow conditions with the same mean velocity and different turbulence intensities. The geometrical and model details conform to the experimental set up of Jordan *et al.* [26] already used for validating the code [16, 17]. For all simulations the rotor was run at a rotational speed $\Omega = 162.3\,\mathrm{rpm}$ and an inflow bulk velocity $\mathrm{U} = 0.33\,\mathrm{m/s}$.

Unsteady computations were carried out using a Cartesian mesh of $2.8 \times 10^6$ mesh points in a domain of size $5.5\,\mathrm{m} \times 1.0\,\mathrm{m} \times 0.6\,\mathrm{m}$, with the finest cell size nearly R/30 in the turbine plane, where R is the rotor radius. From a numerical point of view, a discretization of R/30 has been found sufficient for the LES/ALM simulations [20, 21]. The rotor centre was located at a section 1.5m downstream of the inlet and a height 0.307 m from the bed. For all simulations, the time step was chosen to be $10^{-3}\,\mathrm{R/U}$ and simulations were carried out for a total of $80.41\,s$. The time series are averaged for the last $50\,s$ to avoid the effect of initial transience and obtain stable time-averaged quantities. In regions near the bed and the short cylinder modelling the nacelle, a wall model developed based on Spalding's law [27] is used to avoid using a very fine mesh and increasing computational costs.

For all simulations, the side boundaries are set to periodic conditions. At the inlet, the zero normal gradient is applied for pressure and turbulent inflow conditions are numerically generated using the mapping method. On the downstream boundary, pressure is fixed and the normal gradient of velocity is zero, and the resulting velocity flux through that boundary is adjusted to maintain global continuity. The upper boundary is approximated as an impenetrable, no stress lid, instead of simulating a free surface [28]. No slip condition and zero normal gradient for pressure are applied for the bed boundary and, the short cylinder modelling the nacelle.

### 2.4. Turbulent inflow conditions

In this study, the turbulent inflow conditions are constructed using a modified version of the mapping technique developed by Ahmadi & Tabor for large eddy simulations [29, 30]. As explained in [29, 30], in this method, the velocity a short distance downstream of the inlet to the main domain is sampled and the flow velocity data are reintroduced back into the domain inlet, creating an inlet section integrated into the main domain, in which, variable artificial body forces and velocity corrections are imposed with feedback control to force the flow towards desired mean and turbulent profiles. Using this technique three mean velocity components, u, v and w and three rms velocity components, $\mathrm{u}'$, $\mathrm{v}'$ and $\mathrm{w}'$ are simulated numerically in the inlet section and fed to the main flow.

For this study, the mean and rms velocity components for a turbulent flow in a plain channel are used as the desired mean and turbulent profiles in the mapping technique to generate the inflow conditions. Here, to compare the effect of upstream turbulence on the flow characteristics downstream of the turbine, the experiment developed at the University of Hull is considered as the benchmark [26]. The test case presenting

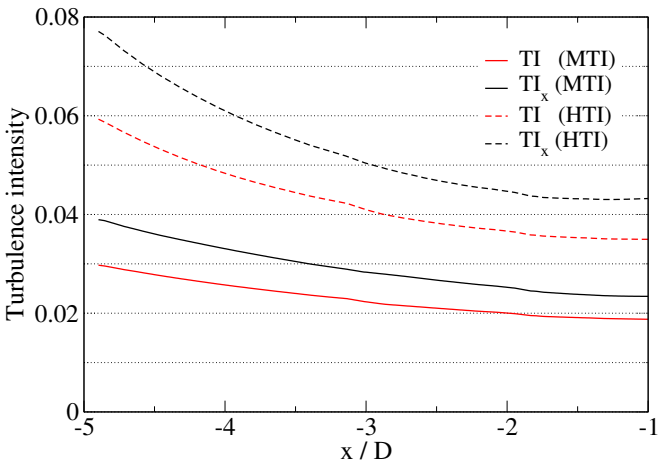


Figure 1: Downstream development of total (TI) and streamwise turbulence ($TI_x$) intensities at the rotor axis height for cases MTI and HTI.

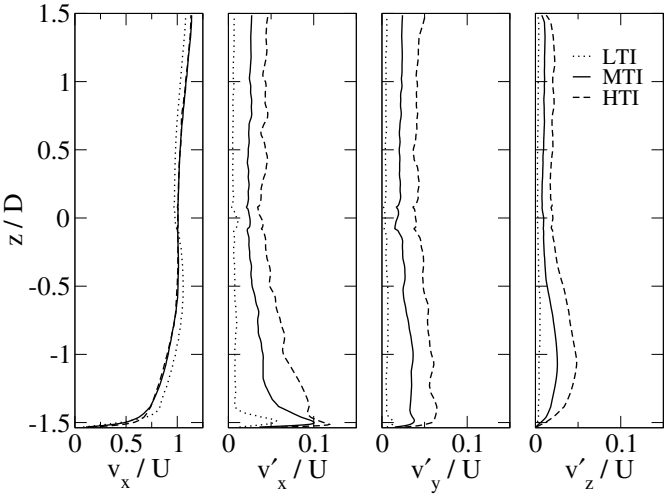


Figure 2: Streamwise mean and rms velocity components at the vertical centre plane of the channel 1D before the turbine plane.

the simulation of the experiment is denoted by MTI. Two other test cases with the same turbine configuration are simulated using the same mean velocity profiles and different turbulence intensities at the inlet; a test case denoted by LTI with a zero turbulence intensity and the second one called HTI with a turbulence intensity twice that of the case MTI. Figure 1 presents the downstream development of total and streamwise turbulence intensities for cases MTI and HTI. The plots show that the turbulence intensity decays with downstream position for both cases but seems to reach a stable condition far from the inlet at a section one diameter (1D) before the turbine plane.

Figure 2 shows the plots of the mean streamwise and three rms velocity components at 1D upstream of the turbine. The profiles for the zero-turbulence (LTI) and high turbulence (HTI) cases are presented by the dotted- and dashed-lines respectively and data for the reference case, MTI, are shown by the solid-lines. The plots show that at a plane 4D downstream of the inlet of the main domain and 1D before the turbine, the mean streamwise velocity profiles are approximately the same for the cases MTI and HTI and they differ a little from that of the case LTI. The ratio between the applied turbulence intensities in the cases HTI and MTI is reduced to nearly 1.9 at this plane. The results for the case LTI show a very low turbulent flow at this location. To have a better view about the effects of the upstream turbulence on the flow structure behind the turbine, the flow properties at this plane are considered as the reference for analysing the flow characteristics downstream of the turbine. The small deviation in the mean velocity profile for the case LTI shown in Figure 2 is ignored. Considering the results in Figure 2, the cases LTI, MTI and HTI are referred to as the low, mid and highly turbulent flows respectively in this paper.

## 3. Results and discussion

The numerical results for the mean velocity components u, v and w, rms velocity components u′, v′ and w′ and turbulent kinetic energy (TKE) are presented and compared for three cases LTI, MTI and HTI. As explained above, the test case MTI presents the numerical simulation of the experiment performed at the University of Hull [26]. Here the corresponding experimental data are also presented to have a better view about the accuracy of the numerical method and results. The numerical results for cases LTI, MTI, HTI and experimental data are presented with black dotted-, solid-, dashed- and red dot-dashed-lines respectively throughout this paper unless stated explicitly otherwise. The quantities are normalised by the inflow bulk velocity and the turbine diameter which are $U = 0.33\,m/s$ and $D = 0.2\,m$ respectively. In all cases, the turbine has a clockwise rotational speed $\Omega = 162.3\,rpm$ when looking downstream. The results are presented along the streamwise direction at the vertical centre plane at two radii 0.98R and 0.82R below the rotor axis starting from 1D before the turbine up to 10D behind it. The experimental data only covers points from the turbine plane up to 5D downstream [26]. Figure 3 shows the position of the turbine in the computational domain and the plane where the experimental data are available. The results are presented at radii 0.98R and 0.82R to investigate the upstream turbulence effects on the wake for two regions; a) around the blade tip, to consider the tip vortices region at 0.98R and b) the inner region of the wake at 0.82R.

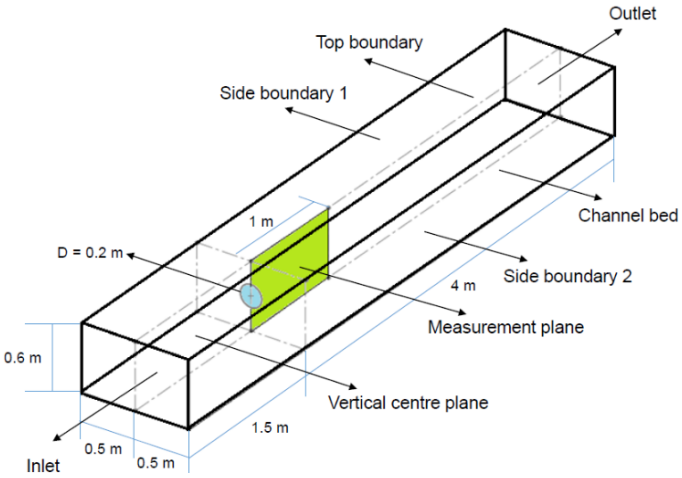


Figure 3: Schematic view of the computational domain.

### *3.1. Mean flow*

Figures 4 and 5 show the mean velocity components in a cylindrical coordinate system along the streamwise direction at Radii 0.98R and 0.82R respectively for the cases LTI, MTI and HTI and the relevant experiment. The top, middle and bottom frames show the velocity deficit and, tangential and radial velocity components respectively.

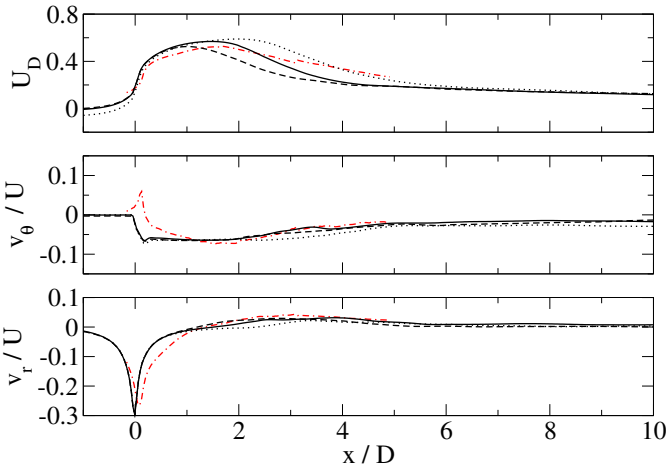


Figure 4: Streamwise velocity deficit and, tangential and radial mean velocity components at the vertical centre plane at radius 0.98R below the rotor axis: LTI (dotted-lines), MTI (solid-lines), HTI (dashed-lines) and Exp. (dot-dashed-lines).

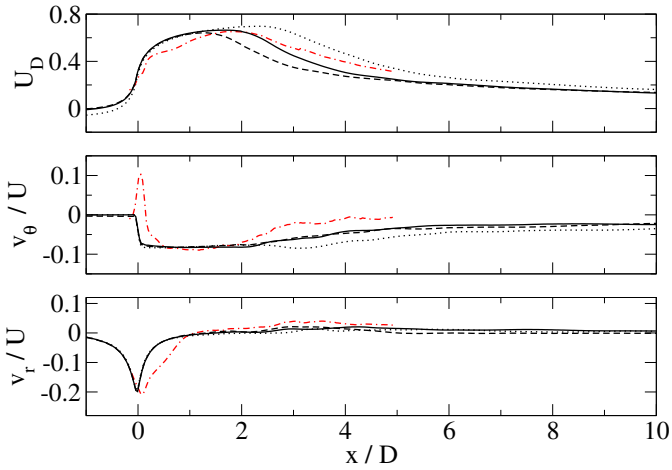


Figure 5: Streamwise velocity deficit and, tangential and radial mean velocity components at the vertical centre plane at radius 0.82R below the rotor axis: LTI (dotted-lines), MTI (solid-lines), HTI (dashed-lines) and Exp. (dot-dashed-lines).

At the first view, the numerical results for the tangential velocity component, $u_\theta$, show a different situation in comparison to the experimental data. While the plots show approximately reasonable numerical results for the streamwise and radial mean velocity components, a large deviation from experimental data is seen for the tangential velocity component around the turbine plane. The experimental data for $u_\theta$ indicates that near the turbine plane the rotor and water rotate in the same direction but further downstream water rotates in the opposite direction as already reported for wind turbines [12, 31, 32]. Since in the ALM technique the blade geometry is not resolved, numerical results do not show the co-rotation region in the flow field.

The plots presented in top frames (Figures 4 and 5) show how the velocity deficit varies longitudinally downstream for the three cases. Velocity deficit is a non-dimensional number normalised relative to the mean speed of fluid approaching the turbine defined as $\mathrm{U_D} = 1 - \mathrm{v_x/U}$. The plots show that there is a reduction in the flow rate when the fluid passes through the turbine and starts to recover further downstream. They show a particularly large flow rate deficit immediately behind the turbine. Figure 4 shows that for each velocity component, the profiles approximately coincide up to a distance around 1.0D behind the turbine for all three cases. Around this location, in the high turbulence case, HTI, the flow structure varies and the wake recovery begins. Variations in the flow structure and wake recovery in the mid-turbulence case, MTI, and low turbulence case, LTI, begin a little later around 1.5D and 2.2D downstream of the turbine respectively. There are similar situations for the velocity profiles at radius 0.82R shown in Figure 5, with a shift downstream around 0.5D in starting variations for the three cases. Although for all cases, the wake is not fully recovered into its initial flow rate at the end of the domain, the cases with higher upstream

turbulence levels show a better wake recovery as depicted in the figures. A comparison reveals that with

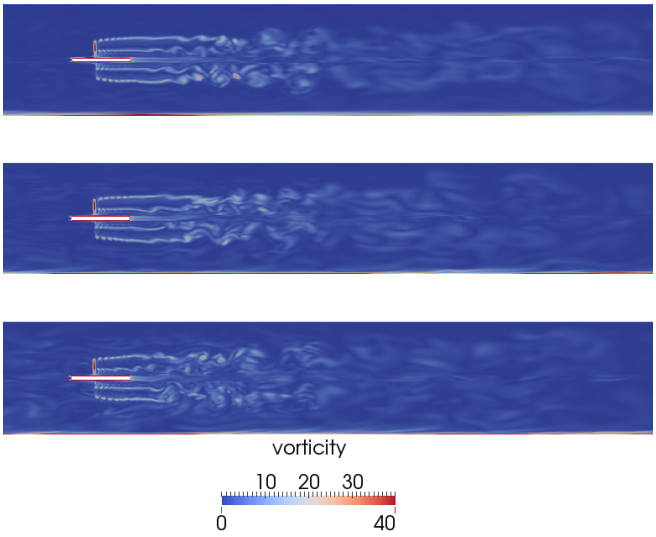


Figure 6: Vorticity at the vertical centre plane of channel for varying levels of inflow turbulence: LTI (top), MTI (middle) and HTI (bottom).

increasing UTI, there is a reduction in the peak value and its location moves towards the turbine plane. These results are consistent with findings reported by Blackmore *et al.* [9]. As explained before, since at a plane 1D before the turbine, the mean streamwise velocity profiles are approximately the same for all cases, therefore the mentioned differences in starting flow regime transition and wake recovery can only be related to the different upstream turbulence levels.

Figure 6 presents an instantaneous snapshot of the vorticity at the vertical centre plane for the three cases. These snapshots provide a qualitative comparison to examine the effects of the upstream turbulence level on starting the tip vortex breakdown and the wake recovery downstream. As Figure 6 shows, with increasing UTI, the wake recovery starts sooner in the line of results shown in Figures 4 and 5.

### *3.2. Turbulent flow field*

The numerical and experimental results for the turbulent kinetic energy (TKE) and rms velocity components in a cylindrical coordinate, $v'_x$, $v'_\theta$ and $v'_r$, at two radii 0.98R and 0.82R below the rotor axis are presented in Figures 7 and 8 respectively.

Figures 7 and 8 show the filtered TKE and rms velocity components, which are the properties of the flow and indicate its turbulence level. By filtering, the Deterministic Velocity Fluctuations (DVFs) caused by the turbine rotation, usually measured in experiments or calculated in numerical simulations, have been removed here. The reason for filtering can be explained by referring to Figure 9. This figure presents the numerical and experimental results for the streamwise rms velocity component at radii 0.98R and 0.82R below the rotor axis

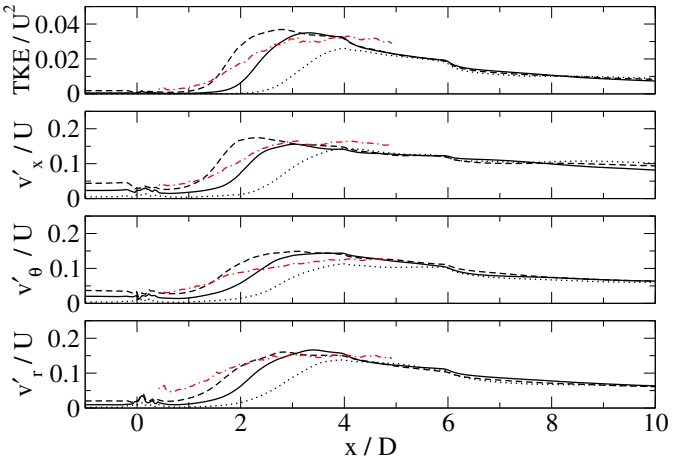


Figure 7: Turbulent kinetic energy and rms velocity components at the vertical centre plane at radius 0.98R below the rotor axis: LTI (dotted-lines), MTI (solid-lines), HTI (dashed-lines) and Exp. (dot-dashed-lines).

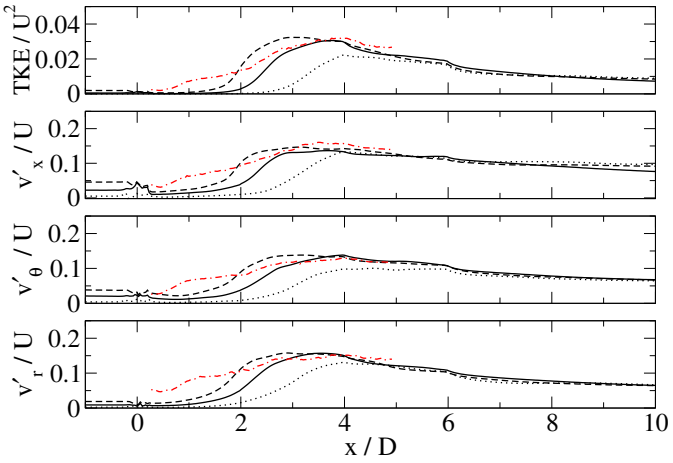


Figure 8: Turbulent kinetic energy and rms velocity components at the vertical centre plane at radius 0.82R below the rotor axis: LTI (dotted-lines), MTI (solid-lines), HTI (dashed-lines) and Exp. (dot-dashed-lines).

before filtering out DVFs. As reported by the author in [17], the occurrence of the first peak in Figure 9 is mainly related to the periodic nature of the flow resulting from the turbine rotation and not to the turbulent fluctuations. In experiments and numerical simulations, the rms velocity component at a point is usually calculated using the time-averaged value of the corresponding velocity component and its standard deviation at the point. This approach is not valid at the turbine plane and a narrow region around it, where the magnitude of velocity at a point, strongly depends on the position of the rotating blades in the turbine plane. Therefore, plotting the results with removing DVFs provides a better view of turbulence characteristics in the near-wake. The filtering process and calculation of DVFs with comparison to experimental data have been presented in detail in [17].

The comparison shows a reasonable agreement between the experimental data and the numerical results obtained for the test case MTI (solid-lines) presented in the figures 7 and 8, particularly in predicting the peak location and its level. The plots depicted in the figures 7 and 8 also indicate that, in a region before the peak location, experimental data shows a higher turbulence level in the flow. This discrepancy can be referred to the mechanical turbulence (the turbulence generated by the blade's boundary layer and vibration) in the real case, which is absent in the numerical simulation due to the nature of the ALM technique used in this study.

Considering the plots depicted for the reference test case, MTI in the figure 7, three regions can be recognised in the flow field. The first region is between the turbine plane up to around 1.5D downstream with a nearly constant turbulence level. The second region is approximately bounded between 1.5D and 3D downstream, where the flow experiences a fast increase in its turbulence intensity. The third region is

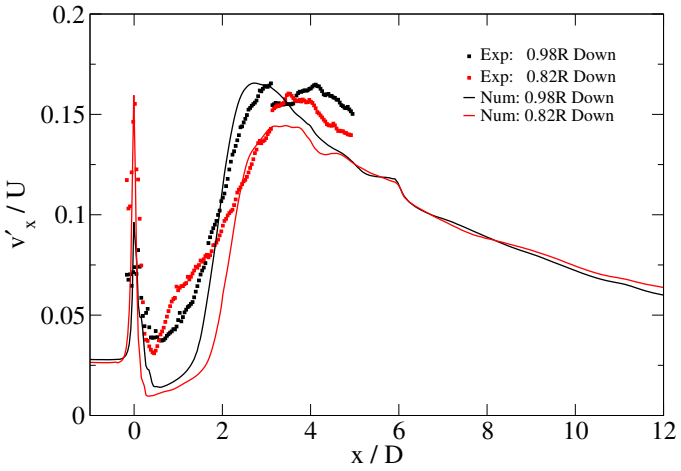


Figure 9: Streamwise rms velocity component at the vertical centre plane at two radii below the rotor axis.

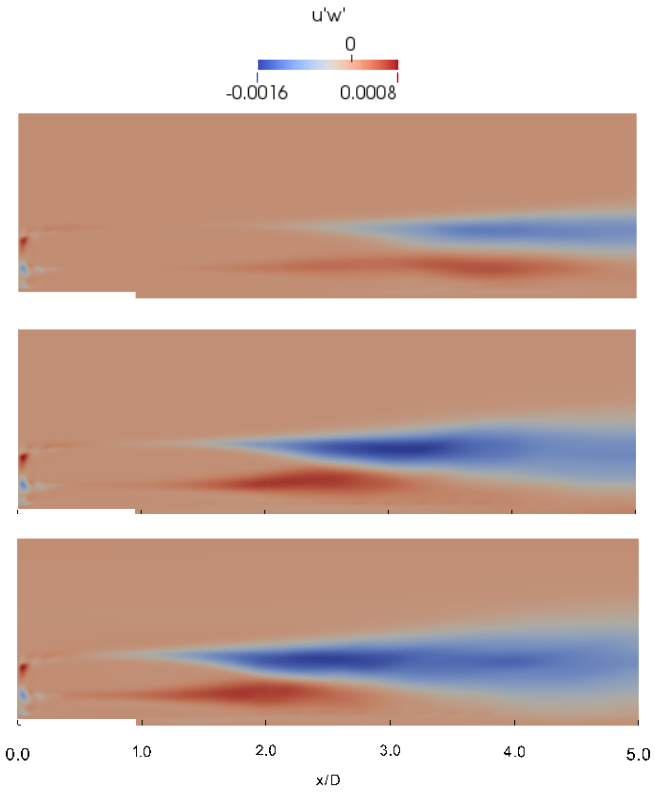


Figure 10: Shear stresses $v'_x v'_r$ at the top half of the vertical centre plane: LTI (top), MTI (middle) and HTI (bottom).

downstream of the peak with a monotonously decreasing behaviour in the turbulence level. Comparing the plots of $v'_x$, $v'_\theta$, $v'_r$ and TKE presented in the figures 7 and 8 for three cases, LTI, MTI and HTI indicates that with increasing UTI, wake instabilities start sooner and the turbulence intensity and TKE peaks shift towards the turbine plane. The comparison also reveals that the shift is accompanied by increases in TI and TKE peak values. Comparing the plots also shows at each frame, three profiles nearly coincide at around 6D and further downstream, which implies that in the far wake, the turbulence and TKE values are independent of the upstream turbulence level. As a possible reason, this situation can be referred to the dominant turbulence in the far wake. Since for all test cases in Figures 7 and 8, the upstream turbulence intensities are much less than the turbulence peak values, thus in the far wake the dominant turbulence is the turbulence generated by the tip vortex breakdown and the influence of UTI is no longer sensible. Of course, at far distances where flows are nearly recovered into their initial conditions the profiles will be recognisable, corresponding to their upstream turbulence levels.

Different regions recognised in Figures 7 and 8 can be distinguished in Figure 10 . This figure depicts shear stresses $v'_x v'_r$ at the top half of the vertical centre plane for three test cases. This is an important quantity mainly associated to the vertical transport of momentum [33, 34, 35], with negative values of shear meaning

the transport from the surrounding flow to the inner wake led to re-energise it [36]. In the near wake region, the shearing stresses are concentrated in a thin sheet at the border of the wake which corresponds to the first region explained above with a nearly constant turbulence level. At the wake border, the shearing stresses are characterised by a negative value (blue color). In the region where the wake instability occurs, the shear stress layer becomes thicker. This region corresponds to the second region distinguished in Figures 7 and 8 where the flow experiences a fast increase in its turbulence level. At each frame, the darkest blue region presents the streamwise location of the turbulence intensity peak shown in Figures 7 and 8, which can be related to the tip vortices breakdown.

The filtered profiles shown in Figures 7 and 8 provide a better view about the characteristics of flow passing the turbine. They show a smooth transmission through the turbine plane. In fact, the turbine rotation just changes the flow direction from parallel to swirling and it does not affect the turbulence level of the flow passing through the turbine. Of course, in a real case, because of the mechanical sources of turbulence which are absent in the ALM technique, there will be an increase in the turbulence level of the flow. This can be seen in Figures 7 and 8 by comparing the numerical results depicted for the MTI case with the presented experimental data.

Although, the main aim of this study is investigating the effects of upstream turbulence intensity on the wake characteristics, comparing experimental and numerical data in Figures 7 and 8 also reveals an interesting point about the influence of mechanical turbulence. A comparison between experimental data and numerical results presented for the case MTI in Figures 7, 8 and 9 shows that despite the higher level of turbulence in the experiment at the region before the peak, the numerical simulation predicts the peak location and its turbulence level with a good accuracy. This implies that the variation of turbulence level inside the wake does not influence the breakdown conditions of tip vortices effectively, which is in contrast to the apparent influence of upstream (ambient) turbulence. Modelling the turbulence generated by rotor blades is an important issue, particularly in numerical simulations such as ALM where the true geometry of the blade is not resolved. Turnock *et al.* [37] and Batten *et al.* [38] have recently used empirical functions to model the mechanical turbulence of tidal turbines; however evaluating the result explained above requires further investigation.

### *3.3. Wake extension*

Figure 10 qualitatively implies that the width of the wake should increase with increasing UTI. To evaluate this point, the shear stresses $v'_x v'_r$ at the upper white border line (the border between brown and blue zones) are plotted in Figure 11 for the three test cases. Solid black, red and green lines represent the upper white border lines in Figure 10 for low, mid and high turbulence cases respectively. As expected, comparing the plots shows that the radial wake extension, resulting from turbulent diffusion of momentum, increases with increasing UTI. In Figure 11 dashed lines represent the wake edges defined where $U_{WE} = 0.95U$ [39] for the three cases. Dashed black, red and green lines represent the wake edges for the cases LTI, MTI and HTI respectively. Comparing the wake edges presented by dashed lines, shows that the width of the wake is

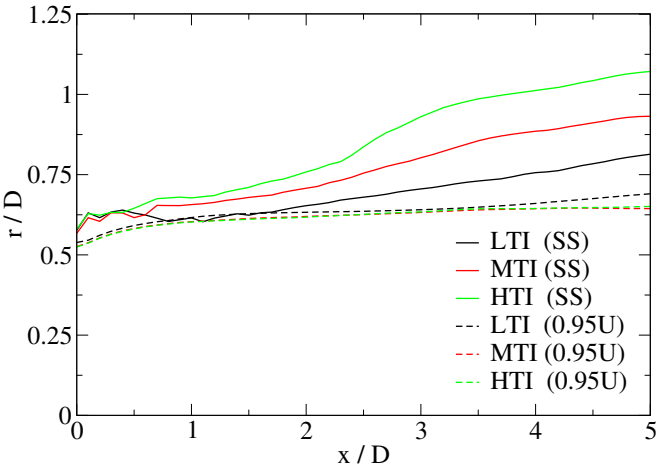


Figure 11: The upper borders of the shear layers shown in Fig. 10 (solid lines) and the wake edges calculated using $U_{WE} = 0.95U$ (dashed lines) at the top half of the vertical centre plane.

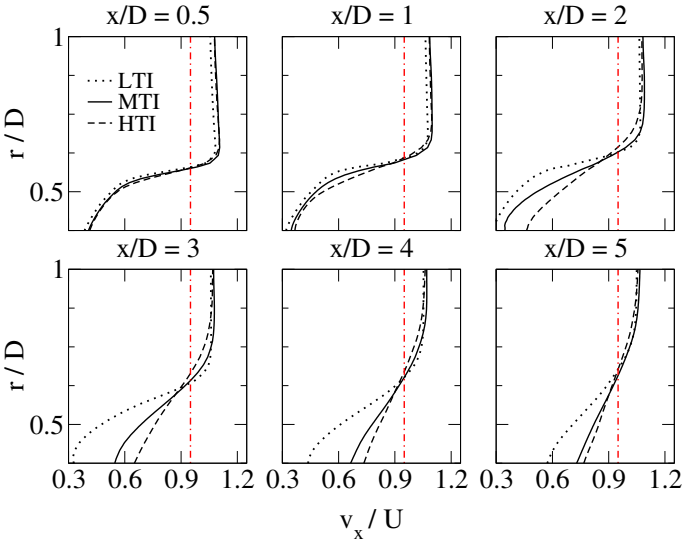


Figure 12: Streamwise mean velocity component at the top half of the vertical centre plane at different downstream locations, dot-dashed lines denote $v_x = 0.95U$.

not significantly affected by increasing UTI. This result is in consistent with findings reported in [9]. The interesting point is that while the streamwise velocity deficit inside the wake, as shown in Figure 5, is strongly affected by increasing UTI, the wake edge is not influenced by that similarly. This situation can be examined by referring to the streamwise mean velocity profiles presented in Figure 12.

Figure 12 depicts numerical results for the streamwise mean velocity component, $v_x$, at the top half of the vertical centre plane at different distances from the turbine plane. As before, black dotted, solid and dashed lines represent results for low, mid and highly turbulent inflow cases respectively. A closer look at the plots shows, at each frame, three velocity profiles approximately intersect at one point meaning the streamwise mean velocity component at this point is not affected significantly by increasing UTI. In all frames, the profiles show that below the intersection point, $v_x$ increases with increasing UTI, which is in agreement with the results presented in Figure 5. An inverse trend is seen for velocity profiles above this point, particularly at locations 2D and beyond.

Apparently the intersection points can be referred to the locations of tip vortices. This opinion implies that tip vortices show a resistance to velocity variations caused by the surrounding flow. In the other words, although there is a radial transport of momentum from the surrounding flow to the inner region of the wake through the tip vortex region, leading to decrease in the velocity deficit in the wake, tip vortices experience no significant variations in the streamwise velocity component, $v_x$. The reduction in velocity deficit with increasing UTI can be explained by referring to Figure 10. As can be seen in the figure, with increasing UTI, the blue region moves closer to the turbine meaning that the radial momentum transport starts sooner, which leads to further increase in $v_x$ in the case with higher UTI. Figure 12 shows that in all frames the

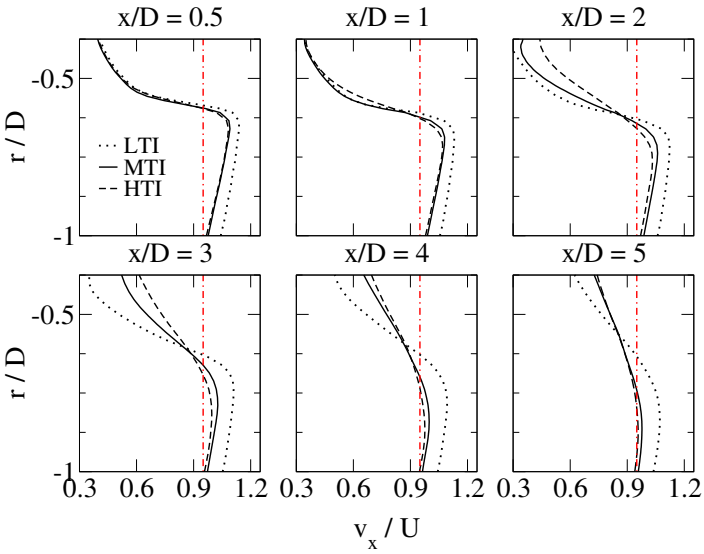


Figure 13: Streamwise mean velocity component at the bottom half of the vertical centre plane at different downstream locations, dot-dashed lines denote $v_x = 0.95U$.

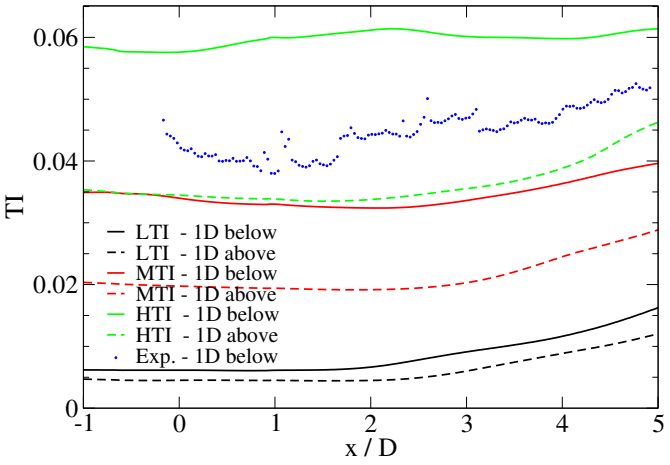


Figure 14: Turbulence intensities at the vertical centre plane below and above the rotor axis.

intersection points are very close to the dot-dashed lines denoting $v_x = 0.95U$, which means the wake edges determined using the relation $U_{WE} = 0.95U$ for low, mid and high turbulence cases should approximately coincide as already seen in Figure 11.

The intersection points explained above are also apparent for the velocity profiles presented in Figure 13. This figure depicts the streamwise mean velocity profiles at the bottom half of the vertical centre plane at different distances from the turbine. As it can be seen in Figure 14, the level of turbulence at the bottom half of the channel is nearly 1.75 times higher than that of the upstream (due to presence of the bed's boundary layer), implying that the intersection points appear for flows with turbulence levels as high as 6% as well. The existence of intersection points at the bottom half of the wake strengthens the idea that these points can be related to the tip vortices locations. As appeared in Figure 13, in contrast to Figure 12, there is a considerable distance between the intersection point and the red dot-dashed line at most frames, leading to different wake widths (determined using the relation $U_{WE} = 0.95U$) for cases LTI, MTI and HTI as shown in Figure 15. Comparing the wake edge plotted for the case MTI in Figure 15 with the wake edge presented for the case HTI in Figure 11, shows why $U_{WE} = 0.95U$ is not the best choice to determine wake edge when investigating the ambient turbulence effects particularly for wall-bounded flows. As can be seen in Figure 14, the turbulence level of the surrounding flow at the bottom half of the case MTI (red solid line) is in the same range as that at the top half of the case HTI (green dash line). But the calculated wake width using $U_{WE} = 0.95U$ at the bottom half of the case MTI (shown in Figure 15)is significantly greater than that at the top half of the case HTI (shown in Figure 11).

Further studies, numerical and experimental, are required to evaluate the existence of the intersection

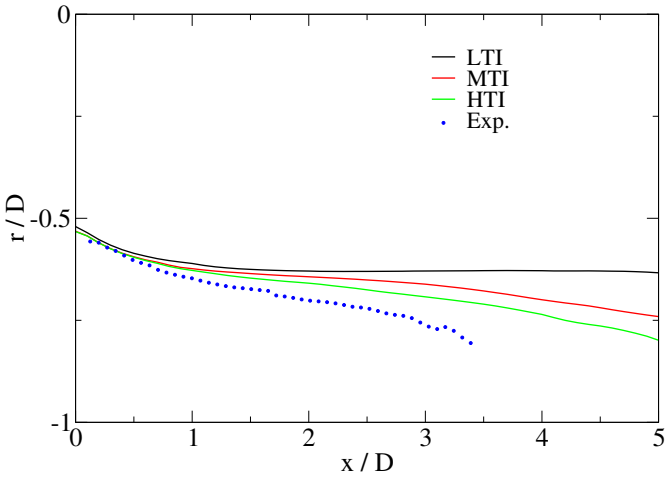


Figure 15: Wake edges calculated using $U_{WE} = 0.95U$ at the bottom half of the vertical centre plane.

points discussed above and their relation to tip vortices. But the numerical results of the present work show that the radial expansion of the inner wake is not affected by the ambient turbulence level. Here "inner wake" stands for the inner region of the wake surrounded by tip vortices. This implies that by increasing the ambient TI, instead of the inner wake, the outer region of the wake bounded by tip vortices and free stream, experiences a radial extension due to the turbulent diffusion of momentum. In the other words, there possibly is a radial transport of tangential momentum from the inner wake to the surrounding flow leading to the radial expansion of the wake. The evaluation of such a process is reserved for future studies. On the other hand, comparing the gap between the intersection point and the red dot-dashed line at each frame of Figure 12 with that at the corresponding frame of Figure 13, indicates a lower streamwise velocity for tip vortices at the bottom half of the channel. This implies the streamwise velocity of tip vortices varies with the normal distance to the bed similar to the vertical variations of streamwise velocity upstream of the turbine, which leads to the asymmetries in the wake.

## 4. Conclusion

The influence of the upstream turbulence intensity on the flow characteristics downstream of a laboratory scale 3-bladed horizontal axis turbine was investigated in this study. Three test cases with the same mean velocity and different inflow turbulence intensities, low, mid and high, were simulated numerically using the hybrid LES/ALM technique. The mean velocity components, velocity deficit, mean turbulent fluctuations and turbulent kinetic energy along the streamwise direction and the wake expansion are compared for three cases.

This study shows that the upstream turbulence level strongly affects the flow characteristics downstream of the turbine by influencing the tip vortices breakdown process. Numerical results indicate that increasing the upstream turbulence intensity brings forward the tip vortex breakdown leading to expedite wake recovery further downstream. The maximum velocity deficit reduces with increasing the upstream turbulence level

and its location shifts towards the turbine plane. Regarding the turbulence intensity along the streamwise direction, an increase in UTI results in increasing the turbulence peak value, and the peak location moves closer to the turbine. Results also indicate the turbulence level in the far wake is almost independent of UTI. Despite the high sensitivity of the tip vortex breakdown process to the upstream/ambient turbulence intensity, numerical results indicate it is not affected significantly by the mechanical turbulence.

The wake extension is the other issue investigated in the present work. The results show there are locations in the flow field where the streamwise velocity is not influenced by the ambient turbulence level. Relating these locations to tip vortices reveals: a) the resistance of tip vortices to the ambient turbulence variations, b) the ambient turbulence level does not affect the radial expansion of the inner region of the wake (the region surrounded by tip vortices), c) in wall-bounded flows, the streamwise velocity of tip vortices varies with the normal distance to the wall corresponding to the variations of streamwise velocity upstream.

Further numerical simulations are currently undergoing to investigate the upstream turbulence effects regarding different integral length scales on the wake characteristics. Future numerical work will focus on investigating the influence of upstream turbulence intensity and integral length scale on the turbine performance with comparison to appropriate experimental measurements.

## Acknowledgements

The author would like to thank Prof. Ping Dong at the University of Liverpool for his great support, Prof. Daniel R. Parsons and his group at the University of Hull for providing the experimental data and Prof. Richard Brown and his group at the University of Strathclyde for providing the blade geometry. This work was funded by the Supergen Marine Challenge Programme of the EPSRC (EP/J010359/1).

## References

[1] L. E. Myers, A. S. Bahaj, R. I. Rawlinson-Smith, M. Thomson, The effect of boundary proximity upon the wake structure of horizontal axis marine current turbines, In Proceedings of the ASME 27th Conference.

[2] F. Maganga, G. Germain, J. King, G. Pinon, E. Rivoalen, Experimental characterization of flow effects on marine current behaviour and on its wake properties, IET Renewable Power Generation 4 (2010) 498–509.

[3] L. E. Myers, A. S. Bahaj, Experimental analysis of the flow field around horizontal axis tidal turbines by use of scale mesh disk rotor simulators, Ocean Engineering 37 (2010) 218–227.

[4] L. Chamorro, C. Hill, S. Morton, C. Ellis, R. Arndt, F. Sotiropoulos, On the interaction between a turbulent open channel flow and an axial-flow turbine, J. Fluid Mechanics 716 (2013) 658–670.

[5] L. Chamorro, C. Hill, V. S. Morton, B. Gunawan, R. E. A. Arndt, F. Sotiropoulos, Effects of energetic coherent motions on the power and wake of an axial-flow turbine, Physics of Fluids 27 (2015) 055104.

[6] P. Mycek, B. Gaurier, G. Germain, G. Pinon, E. Rivoalen, Experimental study of the turbulence intensity effects on marine current turbines behaviour. part I: One single turbine, Renew. Energy 66 (2014) 729–746.

[7] P. Mycek, B. Gaurier, G. Germain, G. Pinon, E. Rivoalen, Experimental study of the turbulence intensity effects on marine current turbines behaviour. part II: Two interacting turbines, Renew. Energy 66 (2014) 876–892.

[8] T. Stallard, T. Feng, P. K. Stansby, Experimental study of the mean wake of a tidal stream rotor in a shallow turbulent flow, Journal of Fluids and Structures 54 (2015) 235–246.

[9] T. Blackmore, W. M. J. Batten, A. S. Bahaj, Influence of turbulence on the wake of a marine current turbine simulator, Philosophical Transactions of the Royal Society A 470 (2014) 1–17 (DOI: 10.1098/rspa.2014.0331).

[10] M. J. Churchfield, S. Lee, J. Michalakes, P. J. Moriarty, A numerical study of the effects of atmospheric and wake turbulence on wind turbine dynamics, Journal of Turbulence 13 (14) (2012) 1–32.

[11] Y. Wu, F. Porte-Agel, Atmospheric Turbulence Effects on Wind-Turbine Wakes: An LES Study, Energies 5 (2012) 5340–5362.

[12] H. Hu, Z. Yang, P. Sarkar, Dynamic wind loads and wake characteristics of a wind turbine model in an atmospheric boundary layer wind, Experiments in Fluids 52 (5) (2012) 1277–1294.

[13] W. Zhang, C. Markfort, F. Porte-Agel, Near-wake flow structure downwind of a wind turbine in a turbulent boundary layer, Experiments in Fluids 52 (2012) 1219–235.

[14] M. Li, S. Radhakrishnan, U. Piomelli, W. R. Geyer, Large eddy simulation of the tidal-cycle variation of an estuarine boundary layer, J. of Geophysical Research 115, C08003.

[15] M. H. B. Ahmadi, P. Dong, Validation of the actuator line method for simulating flow through a horizontal axis tidal stream turbine by comparison with measurements, Renew. Energy 113 (2017) 420–427.

[16] M. H. B. Ahmadi, P. Dong, Numerical simulations of wake characteristics of a horizontal axis tidal stream turbine using actuator line model, Renew. Energy 113 (2017) 669–678.

[17] M. H. B. Ahmadi, The evolution of turbulence characteristics in the near- and far-wake for a horizontal axis tidal stream turbine, submitted to Ocean Engineering, OE-D-17-00226, in revision.

[18] S. Menon, P. K. Yeung, W. W. Kim, Effect of Subgrid Models on the Computed Interscale Energy Transfer in Isotropic Turbulence, Computers & Fluids 25 (2) (1996) 165–180.

[19] OpenFOAM, Released via the OpenFOAM Foundation, See http://openfoam.org.

[20] J. N. Sørensen, W. Z. Shen, Numerical Modelling of Wind Turbine Wakes, Journal of Fluids Engineering 124 (2002) 393–399.

[21] W. Z. Shen, W. J. Zhu, J. N. Sørensen, Actuator Line/Navier-Stokes Computations for The MEXICO Rotor: Comparison With Detailed Measurements, Wind Energy 15 (5) (2012) 811–825.

[22] N. Troldborg, Actuator Line Modeling of Wind Turbine Wakes, PhD Thesis, Technical University of Denmark, Denmark (2008).

[23] L. J. Vermeer, J. N. Sørensen, A. Crespo, Wind turbine wake aerodynamics, Progress in Aerospace Sciences 39 (6–7) (2003) 467–510.

[24] L. A. Martinez, S. Leonardiy, M. J. Churchfield, P. J. Moriarty, A comparison of actuator disk and actuator line wind turbine models and best practices for their use, 50th AIAA Aerospace Sciences Meeting including the New Horizons Forum and Aerospace Exposition 09 - 12 January 2012, Nashville, Tennessee.

[25] L. A. Martinez, S. Leonardiy, Wind Turbine Modeling for Computational Fluid Dynamics, NREL Report NREL/SR-5000-55054, 2013.

[26] L. Jordan, S. Simmons, S. McLelland, D. Parsons, L. Vybulkova, The impact of tidal stream turbines on 3D flow and bed shear stress measured with particle image velocimetry in a laboratory flume, In Proceedings of The 11th European Wave and Tidal Energy Conference (EWTEC) Nantes, France, Sept. 2015.

[27] A. Chaudhari, Large eddy simulation of wind flows over complex terrains for wind energy applications, Ph.D. Thesis, Lappeenranta University of Technology, Lappeenranta, Finland 2014.

[28] C. A. Consul, R. H. J. Willden and S. C. McIntosh, Blockage effects on the hydrodynamic performance of a marine cross-flow turbine, Philosophical Transactions of the Royal Society A 371: 20120299.

[29] M. H. B. Ahmadi, G. R. Tabor, Inlet Conditions for LES using Mapping and Feedback Control, Computers & Fluids 38 (2009) 1299–1311.

[30] M. H. B. Ahmadi, G. R. Tabor, Inlet Conditions for Large Eddy Simulation of Gas-Turbine Swirl Injector, AIAA J. 46 (7) (2008) 1782–1790.

[31] F. Porte-Agel, Y. Wu, H. Lu, R. Conzemius, Large-eddy simulation of atmospheric boundary layer flow through wind turbines and wind farms, J. Wind Eng. Ind. Aerodyn 99 (2011) 154–168.

[32] W. Yuan, A. Ozbay, W. Tian, H. Hu, An experimental investigation on the effects of turbine rotation directions on the wake interference of wind turbines, In Proceedings of the 51st AIAA Aerospace Sciences Meeting Including the New Horizons Forum and Aerospace Exposition Grapevine, TX, USA, 7–10 January 2013.

[33] J. M. Wallace, H. Eckelmann, R. S. Brodkey, The wall region in turbulent shear flow, J. Fluid Mechanics 54 (1972) 39–48.

[34] B. Cantwell, D. Coles, An experimental study of entrainment and transport in the turbulent near wake of a circular cylinder, J Fluid Mech. 136 (1983) 321–374.

[35] R. A. Antonia, L. W. B. Browne, Quadrant analysis in the turbulent far-wake of a cylinder, Fluid Dynamics Res. 2 (1987) 3–14.

[36] N. Hamilton, H. S. Kang, C. Meneveau, R. B. Cal, Statistical analysis of kinetic energy entrainment in a model wind turbine array boundary layer, J. Renew. Sustain Energy 4 (2012) 063105–19.

[37] S. R. Turnock, A. B. Phillips, J. Banks, R. Nicholls-Lee, Modelling tidal current turbine wakes using a coupled RANS-BEMT approach as a tool for analysing power capture of arrays of turbines, Ocean Engineering 38 (2011) 1300–1307.

[38] W. M. J. Batten, M. E. Harrison, A. S. Bahaj, Accuracy of the actuator disc-RANS approach for predicting the performance and wake of tidal turbines, Philosophical Transactions of the Royal Society A 371: 20120293 (2013) 1–14.

[39] R. Malki, I. Masters, A. J. Williams, T. N. Croft, The variation in wake structure of a tidal stream turbine with flow velocity, MARINE 2011, 1–12.